Kinetics and Products of the Reactions BrO + DMS and Br + DMS at 298 K

Trevor Ingham, Dieter Bauer, Rolf Sander, Paul J. Crutzen, and John N. Crowley*

Max-Planck-Institut für Chemie, Division of Atmospheric Chemistry, Postfach 3060, 55020 Mainz, Germany

Received: February 17, 1999; In Final Form: June 9, 1999

The kinetics of the reaction BrO + DMS → products (1), were examined by use of pulsed-laser photolytic generation and time-resolved detection of the BrO radical by absorption spectroscopy at total pressures of 60, 100, and 200 Torr N_2 (1 Torr = 133.322 Pa). A value of $k_1 = (4.40 \pm 0.66) \times 10^{-13}$ cm^3 s^{-1} was obtained independent of pressure at 295 K. This value is significantly higher than that determined previously in low-pressure (<4 Torr He), discharge flow measurements (2.6×10^{-13} cm^3 s^{-1}). By observing the formation of DMSO directly, we obtain a value of 1.17 ± 0.34 for its yield in reaction 1; the major uncertainty is the ±30% in the DMSO cross section. The impact of these results on the chemistry of the remote marine boundary layer was assessed using a chemical box model. At daytime concentrations of 1−2 pmol/mol, the BrO radical was found to be an important sink for DMS and the dominant source of DMSO. In a second set of experiments, pulsed-laser photolysis coupled with resonance fluorescence detection of Br atoms was employed to study the equilibrium kinetics of Br + DMS + M ↔ Br−DMS + M (4, −4) at 100 Torr N_2 and 295 K. Values of $k_4 = (6.36 \pm 0.43) \times 10^{-11}$ cm^3 s^{-1} and $k_{-4} = (1.02 \pm 0.07) \times 10^4$ s^{-1} were obtained, and were used to calculate the equilibrium constant $K_4 = (6.24 \pm 0.56) \times 10^{-15}$ cm^3. The uncertainty is 2σ plus estimated systematic error. At high [Br] ($(1-3) \times 10^{12}$ cm^{-3}), Br atoms are lost from equilibrium via the fast reaction Br + Br−DMS → Br_2 + DMS (5), and a value of $k_5 = (4.2^{+2.3}_{-1.2}) \times 10^{-10}$ cm^3 s^{-1} was obtained. The uncertainty is 2σ plus the major systematic error incurred by estimating $[Br]_o$ from laser fluence measurements. Pulsed-laser photolysis combined with time-resolved UV absorption at selected wavelengths and diode array measurements in the wavelength range 300−450 nm showed a strong absorption centered at 365 nm due to Br−DMS. A value of $\sigma^{365nm}_{max} = (2.74^{+1.6}_{-1.1}) \times 10^{-17}$ cm^2 was obtained by fitting to the time-resolved absorption signal due to Br−DMS. The uncertainty is 2σ plus systematic error (as above).

1. Introduction

Dimethylsulfide (DMS) produced by phytoplankton is the major natural sulfur-containing compound emitted from the ocean.[1] Its oxidation is initiated by the OH radical[2,3,4] and also by the NO_3 radical at night,[2,3] and proceeds via a complex mechanism (see refs.[2,3] for comprehensive reviews), resulting in the formation of aerosols and cloud condensation nuclei[3,5] which can affect the radiative budget of the atmosphere. Reaction with the BrO radical may also be an important degradation process for DMS.[3]

$$\mathrm{BrO} + \mathrm{DMS} \rightarrow \text{products} \qquad (1)$$

Using a value[6] of $k_1 = 2.7 \times 10^{-13}$ cm^3 s^{-1} (current recommendation[7] of $k_1 = 2.6 \times 10^{-13}$ cm^3 s^{-1} at 298 K) and assuming an average BrO mixing ratio of only 0.2 pmol/mol, Toumi[8] calculated that reaction 1 would account for 10% of DMS oxidation globally. Modeling studies[9,10] of the halogen chemistry of both the polluted and remote marine boundary layer (MBL) have identified reactions of HOBr with Cl^- and Br^- in acidified sea-salt particles that generate the photolabile dihalogens Br_2 and BrCl. Both Br_2 and BrCl are photolyzed rapidly to form Br and Cl atoms, resulting in daytime BrO mixing ratios of ≈0.5−5 pmol/mol. At these levels of BrO, reaction 1 will certainly be an important sink for DMS in the MBL.

From the standpoint of reaction kinetics, the trend in the reactivity of XO radicals with DMS is surprising; for ClO[6,11] and IO[6,11−13] the 298 K rate constants are around a factor of 20 lower than for BrO. The previous measurements of k_1 have employed the discharge-flow method, and there is excellent agreement between the reported values at 298 K; $(2.7 \pm 0.5) \times 10^{-13}$, $(2.7 \pm 0.2) \times 10^{-13}$, and $(2.4 \pm 0.6) \times 10^{-13}$ cm^3 s^{-1} by Barnes et al.,[6] Bedjanian et al.,[14] and Le Bras,[15] respectively. Two studies observe a significant negative temperature dependence and quote the following Arrhenius expressions:

$$k_1 = (1.5 \pm 0.4) \times 10^{-14} \exp[(845 \pm 175)/T] \text{ cm}^3 \text{ s}^{-1} \quad \text{(ref 14)}$$

$$k_1 = (9.17 \pm^{2.54}_{2.24}) \times 10^{-14} \exp[(343 \pm 78)/T] \text{ cm}^3 \text{ s}^{-1} \quad \text{(ref 11)}$$

with "activation energies" that differ by over a factor of 2 over the temperature range of about 260 to 340 K. Bedjanian et al.[14] and Barnes et al.[6] also detect the reaction product dimethyl sulfoxide, ($CH_3S(O)CH_3$, DMSO) in close to unit yield. The negative temperature dependence may be indicative of the formation of an association complex which can then decompose either back to reactants or to give products.

$$\mathrm{BrO} + \mathrm{DMS} \leftrightarrow [\mathrm{CH_3S(BrO)CH_3}]^{\ddagger} \rightarrow \text{products}$$

Indeed, reversible adduct formation following the electrophilic addition of the OH radical[16,17] and Br atoms[18] to the sulfur atom in DMS has been observed.

* Author to whom correspondence should be addressed.

10.1021/jp9905979 CCC: $18.00
Published on Web 08/11/1999

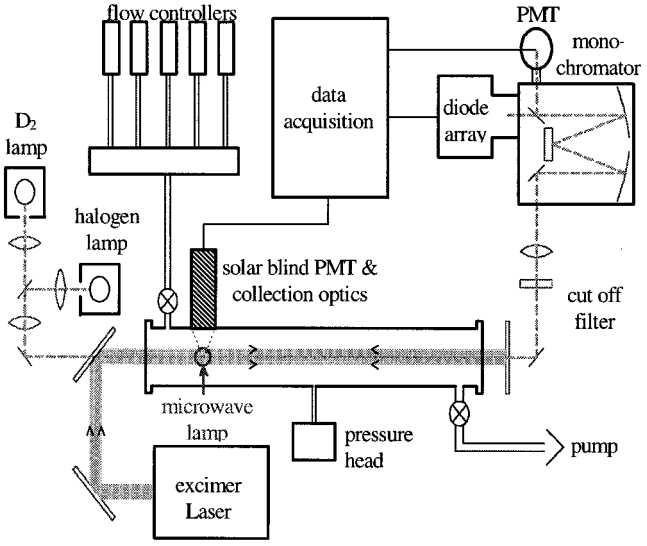

Figure 1. Schematic of the experimental setup. PMT = photomultiplier.

As noted by Bedjanian et al.,[14] the previous low-pressure measurements (<4 Torr He) may underestimate the "true" atmospheric rate constant for BrO + DMS, since thermalization of the association complex may be inefficient. The aim of the present study was to examine the kinetics of reaction 1, by use of laser photolytic generation and time-resolved absorption spectroscopic detection of the BrO radical. Using this method, relatively high pressures of N_2 can be employed and problems associated with the high surface affinity of DMS avoided. In addition, [DMS] can be measured in situ by absorption spectroscopy.

As discussed below, a strong, broad absorption centered around 365 nm has been attributed to the adduct formed by the addition of Br atoms to DMS.[18] Since the present photolytic generation of BrO radicals is accompanied by Br atoms in unit yield, absorption due to the Br−DMS adduct is observed in the present system in the same wavelength range as the BrO vibronic progression. Although we show that the formation of this adduct has no bearing on the value of k_1 determined in this study, we have performed experiments to measure its absorption cross sections, which required prior knowledge of the kinetics of its formation. Experiments were therefore carried out using time-resolved resonance fluorescence monitoring of photolytically generated Br atoms in an excess of DMS.

2. Experimental Section

The pulsed-laser photolysis/UV absorption apparatus (PLP−UV) used in this work has been described elsewhere,[19] although it has been modified to allow detection of atoms by resonance fluorescence (PLP−RF). This system allows the direct, in-situ determination (absorption spectroscopy) of reactant/precursor concentration. Only details relevant to this modification and the present study are given here. All experiments were performed at 295 ± 2 K with N_2 as bath gas.

2.1. PLP−UV. A 1.3 m long cylindrical cell of 5 cm internal diameter equipped with quartz end windows was used as the reaction/absorption/RF cell (Figure 1). Dielectric mirrors enabled the photolysis beam (excimer laser, 248 or 351 nm, 20 ns pulse width) and the analysis light (D_2 lamp) to be overlapped collinearly along the cell's major axis. The excimer laser beam was apertured down to ≈8 mm diameter to reduce any spatial nonuniformities in intensity. The shot-to-shot stability was ≈5%. For 248 nm photolysis of O_3, a further dielectric mirror situated behind the exit window reflected the photolysis beam back through the cell, thus doubling the absorption path length for the generation of radical precursors.

To minimize diffusion, the D_2-lamp analysis beam sampled only a small central section of the volume swept out by the laser. Light from the laser was prevented from entering the monochromator (0.5 m, grating with 300 lines mm^{-1}, detection by diode array and photomultiplier tube) by use of an appropriate filter. The diode array resolution was approximately 1.2 nm, and the wavelength axis was calibrated to an accuracy of 0.3 nm using the emission lines of a Hg Pen-Ray lamp. For the time-resolved absorption measurements of BrO, the entrance and exit slits of the monochromator were set at 0.05 mm, resulting in a resolution of 0.4 nm obtained from the fwhm of an isolated Hg atomic line. For measurements of Br−DMS and DMSO absorption, the slits were increased to 0.25 mm (≈2 nm resolution). I_o was obtained by averaging the PMT signal obtained shortly before the laser pulse, and I_t values were recorded after the laser pulse. The absorption was calculated by use of the relationship $\mathrm{Abs}_t = \ln(I_o/I_t)$.

2.2. PLP−RF. The two orthogonal resonance fluorescence (RF) axes for excitation and collection were situated approximately 10 cm from the entrance to the cell, and were orthogonal to the photolysis axis. The atomic-resonance lamp used to excite fluorescence in photolytically generated Br atoms consisted of an electrodeless microwave discharge through about 3 Torr of a flowing mixture of a trace of Br_2 in He. This was achieved by mixing a flow of 0.005% Br_2 in He with a flow of pure He. The relative amount of Br_2 in the lamp and the total pressure were adjusted to obtain the optimum signal-to-noise ratio. The lamp emission passed through a calcium fluoride filter and through a series of baffles containing a flowing gas filter of 200 Torr cm of methane in N_2. The calcium fluoride and CH_4 filter[20] prevented impurity radiation (from O, H, and N atoms) at wavelengths shorter than 140 nm from entering the cell, but transmitted the strong Br-atom lines between 140 and 160 nm.

Resonance fluorescence was collected via a magnesium fluoride lens (orthogonal to the excitation and laser axes), and directed to the front plate of a solar blind PMT (CsI photocathode). To minimize background scattered light, a Wood's horn was situated at the opposite side of the cell from the lamp. The signals were processed by use of photon counting techniques with multichannel scaling.

For the RF experiments the laser beam was apertured down to a diameter of approximately 4 mm, so that it was just larger than the diameter of the lamp emission at the point of intersection. Under typical flow conditions (see below) it was possible to run the laser at a maximum of 3 Hz so that the photolyzed volume was replenished with fresh reactants prior to the next laser pulse.

Br atoms were generated by the 351 nm photolysis of Br_2 ($\sigma = 3.78 \times 10^{-20}$ cm^2), and the spin−orbit excited-state $Br(^2P_{1/2})$ produced was relaxed rapidly (≈5μs) to the ground state by the addition of 3 Torr of H_2 (reaction 3, $k \approx 6 \times 10^{-12}$ cm^3 s^{-1}).[21]

$$Br_2 + h\nu\ (351\ nm) \rightarrow 2\ Br \qquad (2)$$

$$Br(^2P_{1/2}) + H_2\ (v = 0) \rightarrow Br(^2P_{3/2}) + H_2\ (v = 1) \qquad (3)$$

By use of known concentrations of Br_2 ($1-10 \times 10^{14}$ cm^{-3}) and 351 nm laser fluences (10−60 mJ cm^{-2}; measured in situ by use of a calibrated Joule meter), it was possible to generate known concentrations of Br atoms. The detection limit defined

as $S°/B^{1/2} = 1$ for a 50 ms integration time was determined to be approximately 3×10^9 cm^{-3} (in 100 Torr N_2), where S° is the signal directly after the laser pulse and B is the mean background scattered light signal (obtained by averaging the signal prior to the laser pulse). The decays were corrected for the background signal prior to analysis. The Br-atom resonance signal was shown to vary linearly with [Br] for [Br] $\leq 3 \times 10^{12}$ cm^{-3}; above this value a nonlinearity was encountered due to the reabsorption of fluorescence by Br atoms.[22] It is noted also that there is significant attenuation of the fluorescence signal when [DMS] is present, due to its high absorption cross sections ($\approx 5 \times 10^{-17}$ cm^2)[23] in the wavelength range of the strong Br-atom lines. At the maximum [DMS] (7×10^{14} cm^{-3}) the initial signal was reduced by ≈30%.

The selectivity of the detection system toward Br atoms was tested by generating approximately 10^{12} H, O, and Cl atoms cm^{-3} in 100 Torr N_2 by the 248 nm photolysis of methyl mercaptan (CH_3SH), and the 351 nm photolysis of NO_2 and Cl_2, respectively. Cl atoms are considered since there may be a very small Cl_2 impurity in the Br_2 sample which is used both in the resonance lamp and as a Br-atom precursor. No fluorescence signals were observed for these atoms, and it is thus concluded that the detection is specific to Br atoms.

2.3. Chemicals. Ozone was prepared by use of a commercial ozonizer, and was stored on desiccated silica gel at −78 °C. It was admitted to the cell by passing a flow of N_2 through the storage trap. A flow of Br_2 was generated by passing N_2 over the surface of liquid Br_2 held at ambient temperature in a bubbler. DMS was added by flowing N_2 through a bubbler containing DMS held at −78 °C. Prior to use, the volume of DMS in the bubbler was reduced by about 40% by a flow of N_2 in an attempt to remove any potential minor impurities that were more volatile than DMS. All gas flows were regulated by mass flow meters, and the concentration of the reactants was determined in situ by diode array absorption measurements at 220 nm for DMS ($\sigma = 1.7 \times 10^{-19}$ cm^2)[24] and O_3 ($\sigma = 2 \times 10^{-18}$ cm^2),[7] and at 416 nm for Br_2 ($\sigma = 6.5 \times 10^{-19}$ cm^2).[25] With total pressures of 60, 100, and 200 Torr and flow rates between 5 and 20 L (STD) min^{-1} (slm), the residence time in the cell was about 3 s. For absorption measurements, the time between the laser pulses was always greater than the residence time in order to ensure that the reaction products were removed prior to the next pulse. The stated purities of Br_2, DMS, O_2, H_2, and N_2, were 99.5% (Aldrich), >99% (Aldrich), 99.996% (Linde), 99.996% (Linde), and 99.996% (Linde), respectively.

3. Results and Discussion

3.1. Kinetics of the Reaction of Br Atoms with DMS. Br atoms were produced by the 351 nm photolysis of Br_2 (reactions 2 and 3) in the presence of an excess of DMS ($(0.7-7) \times 10^{14}$ cm^{-3}), in 100 Torr N_2 and 3 Torr H_2. Typically, the initial [Br] ($\approx 1-30 \times 10^{11}$ cm^{-3}) was at least an order of magnitude lower than the [DMS]. The rapid pseudo-first-order [Br] decay to equilibrium (reactions 4, −4) was followed by time-resolved RF with a resolution of 5 μs per channel. Each decay was obtained from the coaddition of 1000−3000 laser pulses.

$$\mathrm{Br} + \mathrm{DMS} + \mathrm{M} \leftrightarrow \mathrm{Br{-}DMS} + \mathrm{M} \qquad (4)$$

Analysis of the flowing DMS/Br_2 mixtures by diode array absorption spectroscopy showed that, under the experimental conditions used for the kinetic and cross section measurements, there was no dark reaction between Br_2 and DMS.

Figure 2 (lower trace) shows an example of a Br-atom decay to equilibrium via reactions 4, −4. In the absence of DMS the diffusion of Br atoms out of the detection volume is slow on this time scale (16 ± 1 s^{-1}). The Br decay was analyzed by use of nonlinear least-squares fitting to the analytical expression (i) for pseudo-first-order decay to equilibrium:

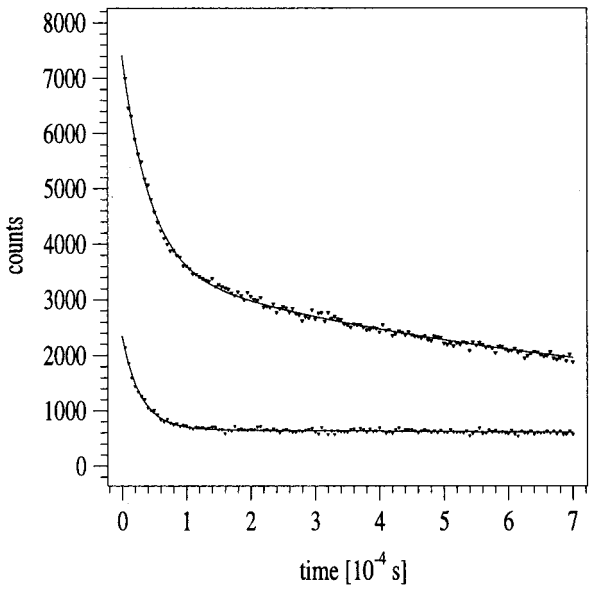

Figure 2. Br-atom decay in the presence of [DMS] = 3.85×10^{14} cm^{-3}. The lower trace is for [Br] ≈ 3×10^{11} cm^{-3} and the solid line is a fit to eq i. The upper trace is for [Br] ≈ 1×10^{12} cm^{-3}, and the solid line is a numerical fit described in the text, (5 μs integration time per channel and 3000 laser pulses gives a total integration time of 15 ms per channel).

$$S_t = S_o \left\{ \frac{k_{-4} + k_f \exp[(-k_f - k_{-4})t]}{k_f + k_{-4}} \right\} \exp[-Dt] \qquad (i)$$

where S_t and S_o are the fluorescence signal at time t and $t = 0$, respectively; k_{-4} is the rate constant for reaction −4; k_f is the pseudo-first-order decay of Br atoms to equilibrium where $k_f = k_4$[DMS]; the final exponential term accounts for the slow diffusion of Br atoms and Br−DMS from the detection zone, where $D \approx 16$ s^{-1}. The rate constant for the addition process (reaction 4) was obtained from a plot of k_f vs [DMS] as shown in Figure 3, where a linear dependence of k_f on [DMS] is observed. A value of $k_4 = (6.36 \pm 0.43) \times 10^{-11}$ cm^3 s^{-1} was obtained from a weighted least-squares fit to the data and $k_{-4} = (1.02 \pm 0.07) \times 10^4$ s^{-1} was obtained from a least-squares weighted average of the values returned from the fitting procedure. The uncertainty refers to statistical scatter at the 2σ level, and includes a systematic error of 3.9% in [DMS] (based upon a measured maximum 3% drift during experiments and 2.5% uncertainty in the cross sections).[24] These values of k_4 and k_{-4} allow us to calculate the equilibrium constant $K_4 = (6.24 \pm 0.60) \times 10^{-15}$ cm^3 at 295 K. This value of K_4 is in good agreement with a value of approximately 5×10^{-15} cm^3 obtained from the data of Wine et al.[18] at the same temperature. The present values of k_4 and k_{-4} are also consistent with those measured by those authors.

Diagnostic tests were carried out which show that there was no influence of laser fluence or photolyte concentration ([Br_2]) on the data obtained for variation of [Br] between 1 and 4×10^{11} cm^{-3}. Variation of the laser repetition rate between 0.5 and 3.1 Hz also had no influence on the measured kinetics.

The behavior described above and exemplified in Figure 2 (lower trace) was observed for initial [Br] in the range $(1-4) \times 10^{11}$ cm^{-3}, where Br atoms decayed to a true equilibrium.

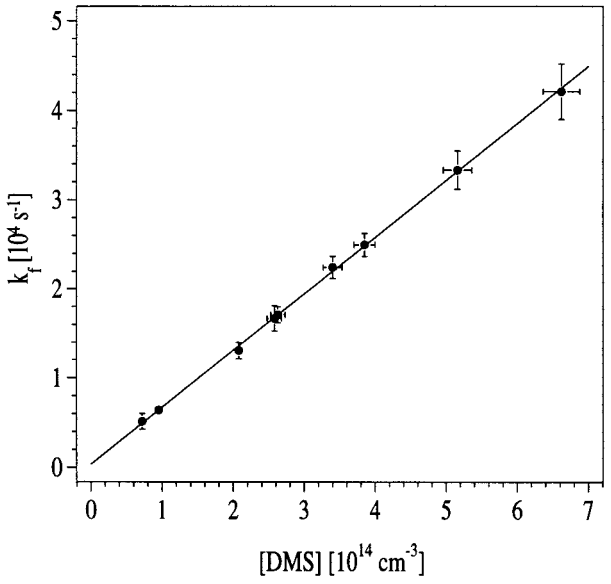

Figure 3. A plot of the dependence of the rate of pseudo-first-order approach to equilibrium on [DMS]. The error bars shown are the 95% confidence limits in k_f returned from the fit, and a 3.9% systematic error in [DMS]. A value of $k_4 = (6.36 \pm 0.43) \times 10^{-11}$ cm^3 s^{-1} was obtained from the weighted fit to these data (95% confidence level).

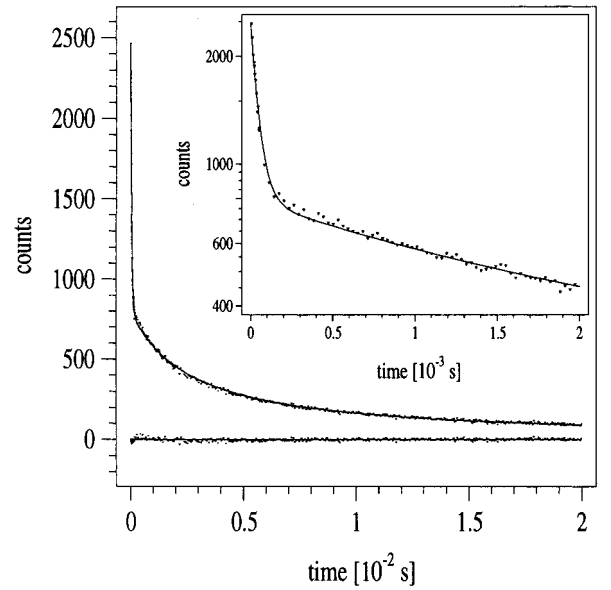

Figure 4. Br-atom decay to equilibrium followed by second-order loss from equilibrium. Initial [Br] and [DMS] were $\approx 1.5 \times 10^{12}$ and 2.4×10^{14} cm^{-3}, respectively. The solid line is a fit and is described in the text; lower trace shows residuals. The insert shows the same data at early reaction times on a logarithmic scale. (5 μs integration time per channel and 1000 laser pulses gives a total integration time of 5 ms per channel.)

However, when the initial [Br] was increased to between 10 and 30×10^{11} cm^{-3} the behavior was distinctly different. Again, rapid decay to equilibrium was observed, but then a slower decay out of equilibrium was observed as shown in Figure 2 (upper trace). As exemplified in Figure 4 for longer reaction times, this slower decay has second-order characteristics. It has been proposed[26] that at relatively high [Br], reaction 5 may occur, which would result in such a decay from equilibrium.

$$\mathrm{Br} + \mathrm{Br{-}DMS} \rightarrow \mathrm{Br_2} + \mathrm{DMS} \qquad (5)$$

Since we know already the rate constants for reactions 4, −4, [DMS], and initial [Br] (see Experimental Section), we employed a numerical integration package[27] to fit the Br-atom decay, with a mechanism I consisting of reactions 4, −4, and (5), with k_5 the only variable parameter. The first-order loss of Br atoms and Br−DMS from the detection volume was fixed at 16 s^{-1}. Figure 4 shows the fit to the Br-atom decay out to 20 ms. The initial [Br] and [DMS] were varied in the range $10-30 \times 10^{11}$ and $(0.7-7) \times 10^{14}$ cm^{-3} respectively, and the Br-atom decays were analyzed as above. No systematic dependence of k_5 on [Br], [DMS], laser fluence, or photolyte concentration was observed. An average value of $k_5 = (4.2^{+2.3}_{-1.2}) \times 10^{-10}$ cm^3 s^{-1} was obtained from 20 data sets. The quoted uncertainty refers to statistical scatter at the 2σ level, and includes a systematic error of 3.9% in [DMS] (see above), and −26%/+53% from estimated uncertainty in $[\mathrm{Br}]_o$. It was possible to measure the laser fluence in situ at the point where the laser beam intersected the emission from the microwave lamp, thus eliminating any systematic error associated with beam divergence. The major contribution to the systematic error in $[\mathrm{Br}]_o$ is a conservative estimate of the accuracy of the Joule meter (±30%).

Reaction 6 is another potential reaction which could produce a decay from equilibrium, and is exothermic by approximately 70 kJ mol^{-1}.

$$2\ \mathrm{Br{-}DMS} \rightarrow \mathrm{Br_2} + 2\ \mathrm{DMS} \qquad (6)$$

Although it was possible to fit the Br-atom decays with a mechanism II including reactions 4, −4, and 6, over the range of [Br] and [DMS] employed, the value of k_6 returned was anticorrelated with [DMS] and varied by over an order of magnitude. If reaction 6 occurred to any significant extent then we would expect to see a dependence of k_5 on [DMS] (with mechanism I), since at higher [DMS] more Br atoms would be tied up in equilibrium as Br−DMS, and reaction 6 should make a greater contribution. Since mechanism I reproduces well the experimental decays over a wide range of conditions and delivers a consistent value of k_5, reaction 5 is considered to be validated, and reaction 6 is at most only a minor process, and we estimate an upper limit of $k_6 < 2 \times 10^{-11}$ cm^3 s^{-1}. This value was obtained by fixing the best fit value of k_5 with mechanism I, and then manually varying k_6 until the fit to the observed decay was just at the limit of the experimental noise. Reaction 6 was not considered in the subsequent analysis of the absorption data used to obtain absorption cross sections for Br−DMS.

Reaction 7 was also considered not to occur.

$$\mathrm{Br} + \mathrm{DMS} \rightarrow \mathrm{CH_3SCH_2} + \mathrm{HBr} \qquad (7)$$

The rate constant for this reaction was measured over the temperature range 386−604 K by Jefferson et al.[28] and extrapolation of the reported Arrhenius expression to room temperature yields a value of $k_7 \approx 3 \times 10^{-14}$ cm^3 s^{-1}. Under the range of [DMS] employed, this value would only produce a first-order loss of Br atoms similar to the rate of diffusion of Br atoms from the detection volume, which is very slow when compared to the observed loss from equilibrium. However, it is noted that at room temperature the dominant reaction of Br atoms with DMS is reversible addition (reactions 4, −4).[18] Since there is a distinct switch in mechanism from abstraction to addition as the temperature is reduced below 310 K,[18] the extrapolation of the high-temperature data should be viewed with some caution.

The rate constant[29] for the recombination of Br atoms (reaction 8) is 2.9×10^{-14} cm^3 s^{-1} at a pressure of 100 Torr

N_2, and shows that this process is unimportant on the time scales employed.

$$Br + Br + M \rightarrow Br_2 + M \qquad (8)$$

From the data of Wine et al.,[18] the enthalpy of formation of the Br−DMS adduct is -60.7 ± 5.0 kJ mol^{-1}, which leads[7] to a ΔH_r for reaction 5 of -131.8 ± 10.9 kJ mol^{-1}. The high value of k_5 can be reconciled with the exothermicity and the weakly bound nature of the Br−DMS adduct. It appears that long-range attractive forces will contribute to stabilization of the transition state, given the expected high polarizability of the S−Br bond and also the polarizability of the nascent Br−Br bond.

3.2. Absorption Cross Sections of the Br−DMS Adduct. With reaction 5 established as the process which removes Br atoms and Br−DMS from equilibrium, it is possible to obtain absorption cross sections for the Br−DMS adduct using PLP−UV if we know the initial [Br] and [DMS]. Unfortunately, due to the nonlinearity in the RF signal above $\approx 3 \times 10^{12}$ cm^{-3}, it was not possible to perform simultaneous RF and absorption measurements, since we required adduct concentrations of at least 5×10^{12} cm^{-3} to obtain reasonable absorption signals for analysis. This required that the initial [Br] was in excess of 5×10^{12} cm^{-3}, at least a factor 2 higher than in PLP−RF measurements, and in the same range as for the BrO + DMS measurements.

To calibrate the adduct absorption cross sections, the initial [Br] had to be known. For this reason, Br atoms formed in the 351 nm photolysis of $\approx 5 \times 10^{15}$ cm^{-3} Br_2, were converted stoichiometrically to BrO radicals in an excess of O_3 (1×10^{15} cm^{-3}). Absorption due to BrO was measured at 338.3 nm and converted to concentration using $\sigma = 1.55 \times 10^{-17}$ cm^2.[30] The O_3 was then replaced with a range of known [DMS], and time-resolved absorption profiles were measured at σ_{max}(Br−DMS) $\approx$ 365 nm.

The Br−DMS absorption signal was then fitted with mechanism I (reactions 4, −4, and 5) as employed above but with k_5 fixed at the value obtained in this work. The only variable parameter was the cross section of Br−DMS at 365 nm. An example of a fit to the Br−DMS absorption signal is shown in Figure 5. At short times, the absorption profile is partially masked by fluorescence from the filter used to prevent laser light entering the monochromator.

[Br] and [DMS] were varied in the range $(0.6-6) \times 10^{13}$ and $(0.7-7) \times 10^{14}$ cm^{-3}, respectively, and an average value of σ_{max}^{365nm}(Br−DMS) $= (2.74^{+1.6}_{-1.1}) \times 10^{-17}$ cm^2 was obtained by fits to 10 data sets. The quoted uncertainty refers to statistical scatter at the 2σ level, and includes an assessment of systematic errors including 3.9% in [DMS] (see above), 10% in the BrO cross section,[30] and −36%/+60% from the respective error quoted for k_5. No systematic dependence of σ_{max}^{365nm}(Br−DMS) on [Br] and [DMS] was observed.

By generating Br atoms as above in the presence of DMS ($(0.7-7) \times 10^{14}$ cm^{-3}), absorption due to the adduct was recorded with a gated diode array detector. Measurements were made over the wavelength range 300−450 nm and comprised of the co-addition of 5000 laser pulses with light intensity recorded 50 ms before the laser pulse (I_o), and the post-photolysis spectra 60 μs after the laser pulse (I_f). The 60 μs delay after firing the laser prevented the detection of fluorescence from the filter. Absorption over a diode array gate time of 100 μs was calculated via the relationship abs $= \ln(I_o/I_f)$.

[Br] was kept at $\approx 6 \times 10^{12}$ cm^{-3} so that absorption changes due to the loss of Br_2 ($\sigma_{max} = 416$ nm) were negligible, i.e.,

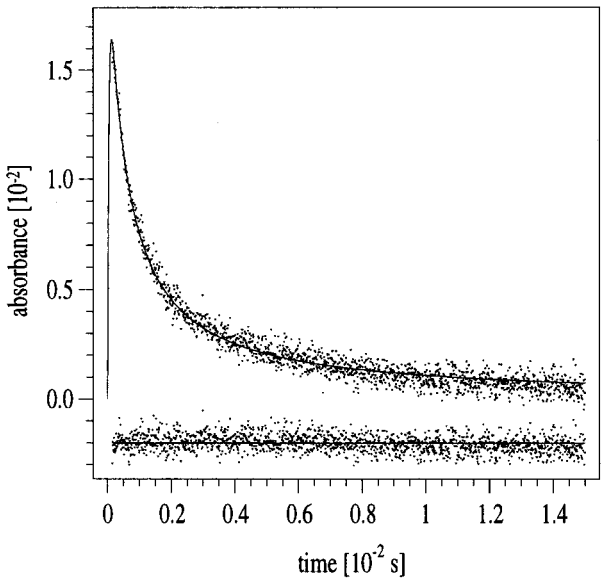

Figure 5. Decay of absorbance due to the Br−DMS adduct at 365 nm. Initial [Br] and [DMS] were 1.1×10^{12} and 2.5×10^{14} cm^{-3}, respectively. The solid line is a fit and is described in the text; lower trace shows residuals. 6000 laser pulses were averaged at 10 μs resolution.

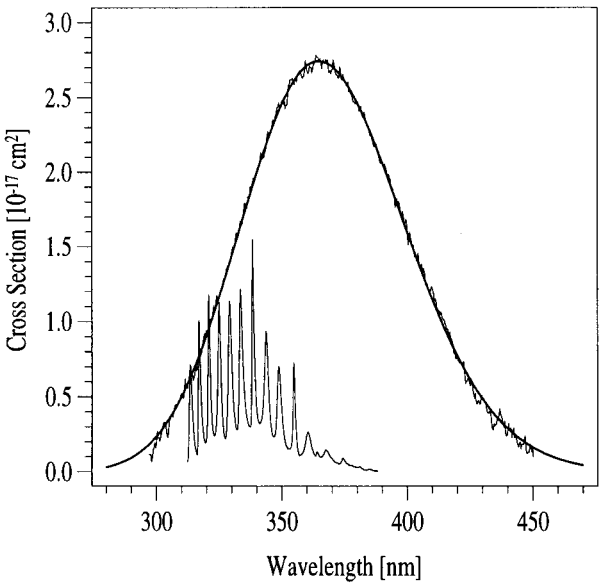

Figure 6. Absorption spectrum of the Br−DMS adduct. The smooth solid line is a fit to a Gaussian function (eq ii). Also shown for comparison is the 298 K BrO cross section data of Wahner[30] (structured line).

maximum Δabs(Br_2) $\approx$ 0.0002. DMS does not absorb in this wavelength range. The spectrum was converted to cross sections by normalizing to σ_{max}^{365nm} obtained as described above. The cross sections of the single absorption band centered at 364.8 nm of the Br−DMS adduct are shown in Figure 6, together with a fit to a Gaussian function (eq ii):

$$\sigma(\lambda) = \sigma_{max} \exp\left\{-FW\left[\ln\frac{\lambda_{max}}{\lambda}\right]^2\right\} \qquad (ii)$$

where $\sigma(\lambda)$ is the cross section at wavelength λ, $\sigma_{max} = 2.74 \times 10^{-17}$ cm^2, and $\lambda_{max} = 364.8$ nm are the cross section and wavelength at maximum absorption, and FW = 64.1 is a width parameter. Figure 6 also shows the 298 K BrO cross section data of Wahner[30] for comparison (see later).

J-value calculations were performed (described elsewhere)[31] which show that the atmospheric lifetime of Br−DMS with respect to photolysis is very short indeed, ranging from ≈ 1.6 s at 15 km and 40° zenith angle to ≈ 3.5 s at the earth's surface at 70° zenith angle.

Since the products of Br−DMS photolysis are almost certainly Br atoms and DMS, even though the photolysis rate of this species is indeed very high, it will have no net effect on the rapid thermal equilibrium (reactions 4, −4) between Br atoms and DMS in the atmosphere.

3.3. Kinetics of Reaction 1. For the kinetic study of reaction 1, BrO radicals were produced by the 248 nm photolysis of O_3 ($(0.5-5) \times 10^{13}$ cm^{-3}) in the presence of Br_2 ($(2-6) \times 10^{15}$ cm^{-3}) and DMS ($(0.5-5) \times 10^{14}$ cm^{-3}) in 60 to 200 Torr N_2 bath gas (reactions 9−11). The bath gas ensured that $O(^1D)$ formed in the photolysis was relaxed in <20 ns to $O(^3P)$ via reaction 10, which is effectively instantaneous relative to the subsequent chemistry. This BrO production scheme results in BrO and Br atoms in approximately the same yield.

$$O_3 + h\nu\ (248\ \text{nm}) \rightarrow O(^3P) + O_2 \qquad (9a)$$

$$\rightarrow O(^1D) + O_2 \qquad (9b)$$

$$O(^1D) + N_2 \rightarrow O(^3P) + N_2 \qquad (10)$$

$$O(^3P) + Br_2 \rightarrow BrO + Br \qquad (11)$$

The rate constant[32] for reaction 11 is 2.0×10^{-11} cm^3 s^{-11} at 298 K, and conditions were selected so that $[Br_2] > [DMS]$ to minimize the loss of O atoms via reaction 12 ($k_{12} = 5.0 \times 10^{-11}$ cm^3 s^{-1}).[7] CH_3 radicals formed in reaction 12 will react rapidly with the excess Br_2 via reaction 13 ($k_{13} = 3.9 \times 10^{-11}$ cm^3 s^{-1}).[33] The fate of CH_3SO in this system is uncertain, but we show later that it has no effect on the value of k_1 obtained in this work.

$$O(^3P) + DMS \rightarrow CH_3SO + CH_3 \qquad (12)$$

$$CH_3 + Br_2 \rightarrow CH_3Br + Br \qquad (13)$$

BrO undergoes rapid self-reaction (reactions 14a, 14b), and a set of experiments was performed to measure the rate constant for this process at 100 Torr.

$$BrO + BrO \rightarrow 2\ Br + O_2 \qquad (14a)$$

$$\rightarrow Br_2 + O_2 \qquad (14b)$$

This serves both as a diagnostic test of our experimental procedure and is necessary as the self-reaction of BrO occurs even in an excess of DMS, and needs to be considered in the kinetic analysis. With the detection wavelength at 338.3 nm, and with $[O_3] = (0.5-5) \times 10^{13}$ cm^{-3} (roughly equal to the initial [BrO]) and $[Br_2] = 6 \times 10^{15}$ cm^{-3}, it was found that it was possible to photolyze most of the O_3 and observe pure second-order BrO decays out to >100 ms. This indicates that there is no observable regeneration of BrO radicals via the reaction of Br atoms (formed in the self-reaction 14a) with O_3 (reaction 15), and that diffusion is unimportant when observing BrO decays.

$$Br + O_3 \rightarrow BrO + O_2 \qquad (15)$$

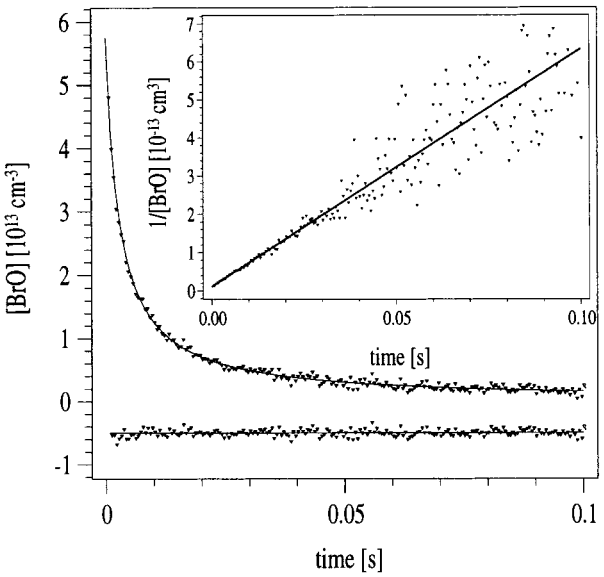

Figure 7. An example of a BrO decay due to the self- reaction 4 only, and a fit to eq iii. The lower trace shows residuals. The insert shows the same data but linearized by plotting inverse concentration. Precursor concentrations: $[O_3] = 6 \times 10^{13}$ and $[Br_2] = 6 \times 10^{15}$ cm^{-3}. Decay obtained from the coaddition of 500 laser pulses at a resolution of 50 μs per channel.

An example of a BrO decay is shown in Figure 7, together with the nonlinear least-squares fit to the integrated form of the second-order eq iii,

$$\frac{1}{[BrO]_t} = \frac{1}{[BrO]_o} + 2k_{14}t \qquad (iii)$$

where $[BrO]_t$ and $[BrO]_o$ are the BrO concentration at time t and $t = 0$, respectively, and k_{14} is the bimolecular rate constant of reaction 14. A value of $k_{14} = (3.11 \pm 0.40) \times 10^{-12}$ cm^3 s^{-1} was obtained from a weighted least-squares average of the individual values returned from the fit. The quoted uncertainty refers to statistical scatter at the 2σ level, and includes a systematic error of 10% in the BrO cross sections.[30] No dependence of k_{14} on laser fluence (30−60 mJ cm^{-2}), initial [BrO] ($(0.5-5) \times 10^{13}$ cm^{-3}), or laser repetition rate (0.1−0.3 Hz) was observed. This value is in excellent agreement with the 298 K literature[7] rate constant of 3.2×10^{-12} cm^3 s^{-1}.

The generation of BrO by this method results in a approximately equal production of Br atoms (reaction 11). As already shown, these react with DMS to form a strongly absorbing adduct (Figure 6) that underlies the vibronic bands of BrO, and is removed rapidly via reaction 5 (Figure 5), and thus contributes most at early reaction times (<4 ms). To overcome this problem when the reaction of BrO with DMS was being studied, differential absorption due to BrO alone was measured by taking back-to-back decays both on the (7,0) band (338.3 nm; $\sigma = 1.55 \times 10^{-17}$ cm^2) and at the minima between the (7,0) and (8,0) bands (337.5 nm; $\sigma = 3.03 \times 10^{-18}$ cm^2).[30] The initial absorption at 337.5 nm was always <50% of that at 338.3 nm. The cross sections employed were taken from the 298 K data of Wahner et al.[30] BrO decays could thus be monitored in the presence of $(0.5-5) \times 10^{14}$ cm^{-3} DMS. One measurement consisted of the coaddition of 200−500 laser pulses.

In these experiments, the maximum loss of O atoms via reaction with DMS (reaction 12) was approximately 15%. It was not possible to increase the Br_2 concentration further to suppress reaction 12 because we observed a dark reaction

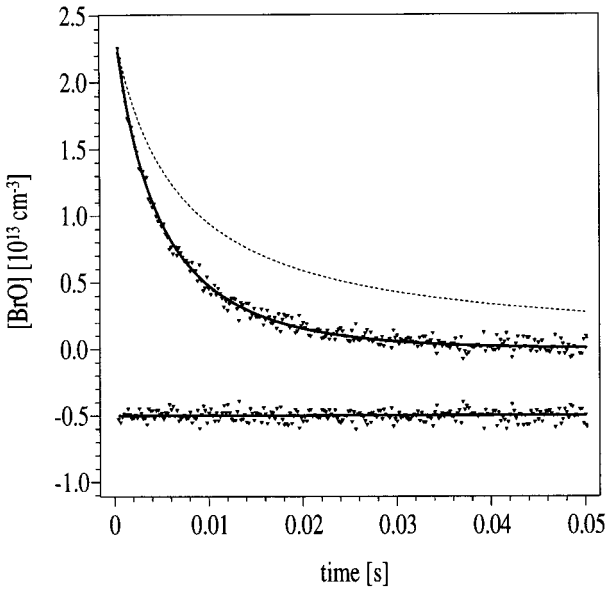

Figure 8. An example of a BrO decay in the presence of DMS, and a fit to eq iv (solid line). The lower trace shows residuals offset for clarity. Also shown is a calculated BrO decay (broken line) which would occur in the absence of DMS. Precursor concentrations: $[O_3] = 2.5 \times 10^{13}$, $[Br_2] = 6 \times 10^{15}$, $[DMS] = 2.5 \times 10^{14}$ cm^{-3}. 500 laser pulses were averaged at a resolution of 100 μs.

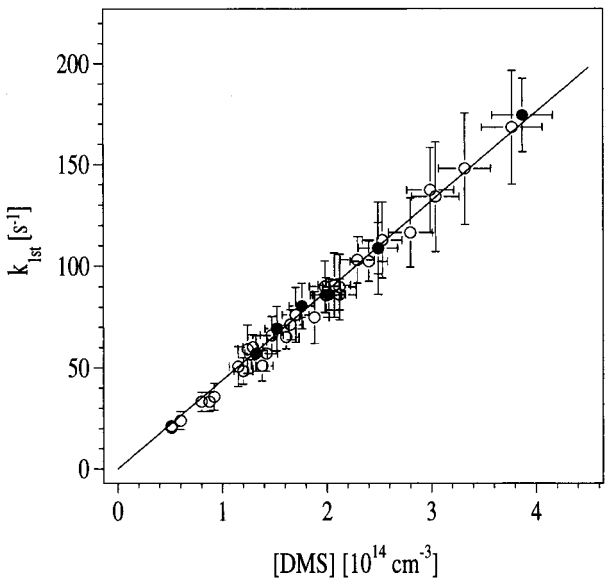

Figure 9. A plot of the first-order component of the BrO decay (k_{1st}) vs [DMS] at 295 ± 2 K and 100 Torr. The solid line is a weighted least-squares fit to the data. The error bars shown are the 95% confidence limits in k_{1st} obtained from the fitting procedure, and a 7.4% systematic error in [DMS]. The open circles are for $[Br_2] = 6 \times 10^{15}$ cm^{-3} and the filled circles are for $[Br_2] = 2 \times 10^{15}$ cm^{-3}. A value of $k_1 = (4.40 \pm 0.22) \times 10^{-13}$ cm^3 s^{-1} was obtained from a weighted least-squares fit to all the data (95% confidence level).

between Br_2 and DMS when $[Br_2]$ was increased to around 10^{16} cm^{-3}. This also precludes increasing [DMS] to force reaction 1 and minimize loss of BrO via reaction 14. It is believed that this dark reaction forms a charge-transfer complex (Br_2−DMS).[34] At significantly higher Br_2 and DMS concentrations (>10^{16} cm^{-3}), a yellow compound (thought to be bromosulfonium bromide)[34] was observed at the mixing point and disappeared over a few minutes when the Br_2 and DMS were excluded from the flow. It should be noted that under the conditions employed throughout the kinetic measurements no dark reaction between Br_2 and DMS was observed. This was confirmed by diode array spectroscopic analysis of the flowing mixtures, whereby the concentration of DMS was unaffected by the addition of the excess Br_2. Furthermore, a similar test confirmed that there was no observable dark reaction between O_3 and DMS.

Under the experimental conditions selected (see above) where [DMS] was always greater than a factor of 10 higher than $[BrO]_o$, there is a contribution to the BrO decay due to reaction 14, and therefore the decays were analyzed as mixed first- and second-order kinetics by use of nonlinear least-squares fitting to eq iv:

$$\frac{1}{[BrO]_t} = \left\{\left(\frac{1}{[BrO]_o} + \frac{2k_{14}}{k_{1st}}\right)\exp(k_{1st}t) - \left(\frac{2k_{14}}{k_{1st}}\right)\right\} \quad \text{(iv)}$$

where $[BrO]_t$ and $[BrO]_o$ are the BrO concentration at time t and $t = 0$, respectively, k_{14} is the rate constant for reaction 14, and k_{1st} is the pseudo-first-order decay rate, where $k_{1st} = k_1[DMS]$. For all fits, the value of k_{14} was fixed at the value measured in this work. Figure 8 shows an example of a BrO concentration−time profile, and a fit to eq iv. Also shown for comparison is a calculated BrO decay in the absence of DMS. As confirmed above, with the low $[O_3]$ employed throughout this study, the regeneration of BrO (reaction 15) from the Br atoms formed in reaction 1 and in the BrO self-reaction 4a was unimportant.

The rate constant for reaction 1 was obtained from the slope of a plot of the first-order component of the overall BrO decays (k_{1st}) vs [DMS]. Figure 9 shows the expected linear dependence of k_{1st} on [DMS] and the zero intercept. The open circles are for measurements with the excess $[Br_2] = 6 \times 10^{15}$ cm^{-3}. As the [DMS] is increased, a greater proportion of the O atoms produced in the photolysis of O_3 react with DMS (reaction 12). With [DMS] at the maximum value and $[O_3] \approx 2.5 \times 10^{13}$ cm^{-3}, approximately 15% of the O atoms react with DMS to form a maximum of ≈ 3.7×10^{12} cm^{-3} CH_3SO. Since the linear dependence of k_{1st} on [DMS] is not affected by this, it is assumed that the formation of CH_3SO does not measurably affect the decay rate of BrO. To confirm this, the initial $[Br_2]$ was reduced to 2×10^{15} cm^{-3} to enhance the possible contribution from this secondary chemistry, such that a maximum of ≈33% of the O atoms reacted with DMS to form ≈8.2×10^{12} cm^{-3} CH_3SO. The [DMS] was corrected accordingly (<3%), and as shown in Figure 9 (filled circles), no contribution from this secondary chemistry is observed.

A value of $k_1 = (4.40 \pm 0.66) \times 10^{-13}$ cm^3 s^{-1} was obtained at 295 K and 100 Torr from a weighted least-squares fit to all the data in Figure 9. The uncertainty quoted refers to statistical scatter at the 2σ level and includes an assessment of systematic errors including 7.4% in [DMS] (based upon a measured maximum of 7% drift during experiments and 2.5% uncertainty in the cross sections).[24] To assess the effect due to the 10% uncertainty in the BrO cross sections[30] we recalculated and refitted every BrO concentration−time profile with the differential cross section increased and decreased by 10%. The effect of this on the rate constant obtained from plots of k_{1st} vs [DMS] was ± 5%.

Tests were performed to see if k_{1st} was influenced by the initial BrO concentration. With [DMS] and $[Br_2]$ fixed at 2.1×10^{14} and 6×10^{15} cm^{-3} respectively, the $[O_3]$ was held at approximately 0.5, 1, and 2×10^{13} cm^{-3}. Thus it was possible to vary the initial [BrO] over a similar range as the $[O_3]$. No systematic dependence of k_{1st} on initial [BrO] was observed, thus confirming that the first- and second-order components of the BrO decay were separated reliably. Considering all the

measurements shown in Figure 9, when we divide the data into two sets where the initial [BrO] is <1.3 and $>1.6 \times 10^{13}$ cm^{-3}, the values of k_1 obtained from the slopes of plots of k_{1st} vs [DMS] are not separable statistically at the 2σ level. Thus, the value of k_1 obtained is independent of initial [BrO]. This diagnostic test also serves to confirm there is no detectable influence of the Br−DMS adduct on k_1, since variation of $[BrO]_o$ results in a similar variation in [Br], and thus [Br−DMS] (see later).

To test for any pressure dependence in the rate constant, experiments were repeated at 60 and 200 Torr. Initial experiments at 60 Torr with the BrO self-reaction showed that diffusion was unimportant in the first 40 ms, and we only analyzed the data out to this time; this time period encompassed $>80\%$ of the total BrO decay. With $[Br_2]$ held at 6×10^{15} cm^{-3} and [DMS] varied as above, values of k_1 of $(4.40 \pm 0.60) \times 10^{-13}$ and $(4.36 \pm 0.65) \times 10^{-13}$ cm^3 s^{-1} were obtained at 60 and 200 Torr, respectively, and show that there is no measurable pressure dependence over this range. Again, a linear dependence of k_{1st} on [DMS] was observed with zero intercepts. The uncertainty quoted is as described above, and the values of k_1 at each pressure are not statistically separable at the 2σ level.

Diagnostic tests were performed which showed that there was no influence of laser fluence ($\approx$30−60 mJ cm^{-2}) or repetition rate (0.3−0.1 Hz) on the value of k_1 obtained. The independence of k_1 on laser fluence confirms that there was no measurable influence of the photolysis of DMS at 248 nm ($\sigma = 1.28 \times 10^{-20}$ cm^2). On consideration of the respective experimental uncertainties, the value of the rate constant for reaction 1 determined in this work is significantly higher than all of the previous determinations at low pressures of He. This is consistent with the proposed mechanism of reaction 1, which may require thermalization of the association complex prior to product formation. Further, this work supports the "high" value of the rate constant relative to the analogous reactions of ClO and IO with DMS.

The formation of the Br−DMS adduct is the greatest potential complication in this study (both optically and perhaps chemically), and we tested further the possibility that a reaction such as (reaction 16) can lead to an over-determination of k_1. The potential reaction 16 of BrO with Br−DMS is exothermic by about 70 kJ mol^{-1} if the reaction proceeds via Br-atom exchange (reaction 16a), and exothermic by about 260 kJ mol^{-1} if the products are Br_2 and DMSO (reaction 16b).

$$BrO + Br{-}DMS \rightarrow Br_2O + DMS \quad (16a)$$

$$\rightarrow Br_2 + DMSO \quad (16b)$$

We have presented experimental evidence to suggest that reaction 16 does not occur to any significant extent (also numerical simulation requires only reactions 1 and 14 to fit the experimental BrO decay data, and returns values of k_1 in excellent agreement with that obtained via plots of k_{1st} versus [DMS]). To test this further, a reaction system including reactions 4, −4, 5, 14, and reactions 1 and 16 was modeled. We fixed the values of the rate constants determined in this work, other than k_1 which was fixed at the recommended[7] value 2.6×10^{-13} cm^3 s^{-1}, and allowed k_{16} to vary to fit the BrO decays. The initial [Br] was equated to the initial [BrO] obtained from the analytical analysis. It was not possible to reproduce the experimental decays, since reaction 16 introduces excessive second-order character at early reaction times. We show later that the majority of the Br−DMS had been removed in <2 ms, and therefore did not exist long enough to significantly perturb the much slower BrO decay as shown in Figure 8. The data in Figure 8 also show that we could separate reliably the absorption due to BrO and Br−DMS in the first 2 ms where the maximum absorption due to Br−DMS occurs.

Although $[O_3]$ is low, we considered also the potential reaction of Br−DMS with O_3 (reaction 17) (exothermic by about 68 kJ mol^{-1}) which would be most important at early reaction times before the Br−DMS is removed, and would be a secondary source of BrO. This process can also be ruled out as the experimental profile of BrO (see residuals at early reaction times in Figure 8) is not consistent with the occurrence of this reaction. Additionally, the Br−DMS profile in the presence and absence of O_3 is unaffected, i.e., we can fit the profiles well with the mechanisms described in the text with no evidence of systematic errors in the chemistry involved.

$$O_3 + Br{-}DMS \rightarrow BrO + O_2 + DMS \quad (17)$$

3.4. Products of Reaction 1. Reaction 1 is exothermic by $\approx$128 kJ mol^{-1} if the products are DMSO and Br atoms. The formation of weakly bound adducts between OH radicals, and Br atoms with DMS is exothermic[18,35] by around 40−60 kJ mol^{-1}. Assuming a similar bond strength in the BrO−DMS intermediate, then thermal decomposition back to reactants may be expected. The present value of k_1 has been shown to be independent of N_2 pressure from 60 to 200 Torr, which indicates that the association complex is thermalized under these conditions. However, the overall effect in k_1 of varying pressure from <4 Torr He to 60−200 Torr N_2 is less than a factor of 2.

Previous low-pressure measurements determined the products of reaction 1 as DMSO and Br atoms[11,14] in approximately unit yield, and experiments were carried out to check this at higher pressures. In the first set of experiments, we measured absorption due to the formation of DMSO directly at 210 nm ($\sigma = 8.2 \times 10^{-18}$ cm^2).[36] Experiments were performed with the same methodology as the kinetic study of reaction 1 where a differential decay due to BrO alone was recorded, and then the monochromator was shifted to 210 nm and the slit width was increased to 0.25 mm since the DMSO spectrum is unstructured. Initial experiments under conditions designed to maximize DMSO formation ($[BrO]_o \approx 4 \times 10^{13}$, [DMS] $\approx 4 \times 10^{14}$, and $[Br_2] = 6 \times 10^{15}$ cm^{-3}) showed there was an initial positive contribution to the absorption profile at 210 nm prior to the rise of DMSO, which was $\approx$20% of the maximum absorption. When the Br_2 was removed from the system so that all the O atoms reacted with DMS (reaction 12), the magnitude of this absorption increased and was characteristic of the rapid (<50 μs) formation of a stable species with no detectable self-reaction. Further, the magnitude of the absorption was consistent with the loss of O atoms by reaction with DMS relative to reaction with Br_2. The stable species is most likely CH_3SO,[7] but was not investigated further since its contribution to the absorption profile was reduced considerably by selecting conditions where virtually all ($>97\%$) the O atoms reacted with Br_2 ($[BrO]_o \approx 10^{13}$, [DMS] $= 1 \times 10^{14}$, and $[Br_2] = 9 \times 10^{15}$ cm^{-3}).

To confirm that the absorption was due to DMSO, diode array measurements were made over the wavelength range 200−240 nm at various delays after the laser pulse (1 to 50 ms) with a gate time of 5 ms. The spectra obtained were in good agreement with the DMSO spectrum of Hynes and Wine.[36]

Figure 10 shows an example of time-resolved measurements of the BrO decay and the DMSO rise. The solid line is a numerical fit to the BrO decay with a mechanism including reactions 1 and 14; k_{14} was fixed at the value determined above,

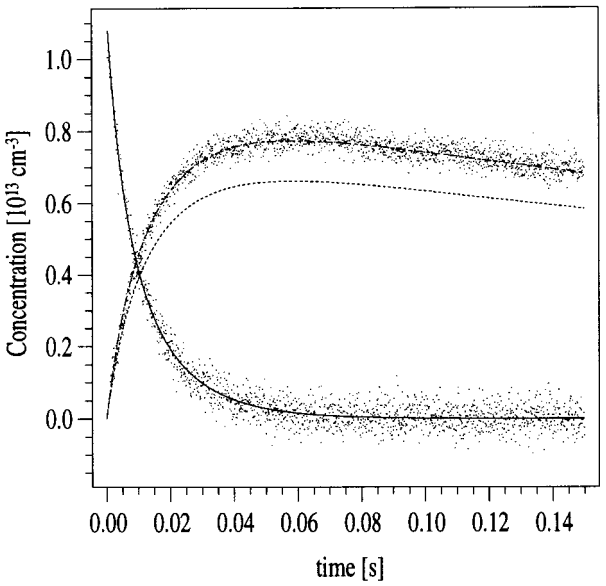

Figure 10. An example of the decay of BrO and the rise of DMSO. The solid line is a numerical fit to the BrO decay and the broken line is the predicted rise of DMSO. The dashed line is the predicted DMSO rise scaled to fit the experimental DMSO rise (data points). $[BrO]_o = 1 \times 10^{13}$, $[Br_2] = 9 \times 10^{15}$, and $[DMS] = 1 \times 10^{14}$ cm^{-3}. There is ≈ 30% loss of BrO via reaction 15, and at later reaction times the effects of diffusion and cell flow-out are observed and account for a loss rate of ≈ 1.7 s^{-1}. 500 and 1500 laser pulses were averaged to obtain the BrO decay and DMSO rise, respectively, at a resolution of 100 μs.

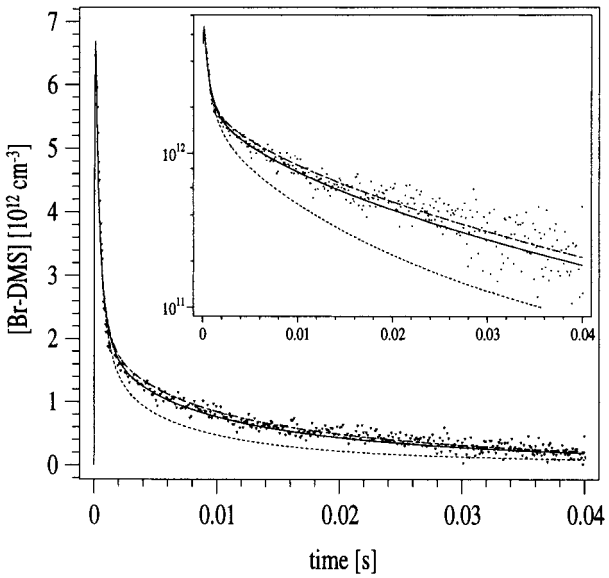

Figure 11. An example of the temporal profile of [Br−DMS] in the BrO + DMS system, for initial $[Br] \approx [BrO] = 1.5 \times 10^{13}$ and $[DMS] = 2.1 \times 10^{14}$ cm^{-3}. The insert shows the same data on a logarithmic scale. The lines shown are the result of fits to the Br−DMS absorption signals where the Br-atom yield from reaction 1 was fixed at (i) unit yield (dashed line), (ii) 0.7 yield (solid line), and (iii) no Br-atom formation (broken line). The data were obtained from the coaddition of 1500 laser pulses from three separate experiments, with time resolutions of 20 and 100 μs for the first 50 and next 400 channels, respectively.

and $k_1 = (4.21 \pm 0.18) \times 10^{-13}$ cm^3 s^{-1} was returned from the fit (2σ error), in good agreement with the value obtained above. The broken line is the predicted rise of DMSO assuming unit yield of DMSO in reaction 1, and indicates that under the conditions selected there is ≈30% loss of BrO via its self-reaction 4. The absorption profile at 210 nm was corrected (≈20%) for the loss of DMS via reaction 1 prior to calculating the DMSO concentration via the Beer−Lambert relationship. This was done by calculating the DMS loss profile in the numerical fitting procedure, and converting it to absorption via the known cross section at 210 nm ($\sigma = 1.73 \times 10^{-18}$ cm^2).[24] The fit to the data points (dashed line) was obtained by scaling the predicted DMSO profile. At later reaction times the effects of diffusion and cell flow-out are observed and account for a loss rate of ≈1.7 s^{-1}. The experimental DMSO profiles display the same kinetic behavior as that predicted by numerical integration, thus indicating that the DMSO is formed via reaction 1. A value of 1.17 ± 0.34 was obtained for the yield of DMSO via reaction 1. The uncertainty refers to statistical scatter at the 2σ level, and includes an assessment of systematic errors including 30% in DMSO cross section,[36] 10% in BrO cross section, and 7.4% in [DMS] (see above). We conclude that DMSO is the major product of reaction 1, but given the uncertainty in the DMSO cross section, this result implies a lower limit of 0.83 for the DMSO yield, and the possibility of other minor product channels cannot be excluded (see below).

In additional experiments, an indirect method was employed whereby the temporal profile of Br−DMS was used as a spectroscopic marker for Br atoms (the coproduct of DMSO in reaction 1) in this system. As described in section 3.1, we determined the rate constants for the equilibrium process (reactions 4, −4), and reaction 5 which produces loss from equilibrium, and also the cross sections for Br−DMS. As mentioned above, there is evidence which rules out a significant interaction of BrO with Br−DMS. Thus the temporal profile of Br−DMS in the BrO + DMS system is controlled by the same processes as described in section 3.1, the only additional processes are the formation of Br atoms via reactions 1 and 14a. If this is the case, then we should be able to describe the kinetics of Br−DMS formation and loss with reactions 4, −4, 5, and reactions 1 and 14 which produce Br atoms over a longer time period than the instantaneous production of Br atoms from the BrO source chemistry.

To measure time-resolved absorption profiles of Br−DMS the following approach was adopted. First, differential absorption measurements were performed at 338.3 and 337.5 nm to obtain the initial concentration of BrO (reaction 11; and thus Br atoms). Then the monochromator was shifted to 390 nm where Br−DMS absorbs (see Figure 6) but BrO does not. As the Br−DMS spectrum is unstructured, it was possible to increase the width of the monochromator slits to obtain improved signals. Time-resolved absorption measurements were then performed for a range of initial $[BrO] \approx [Br]$ ($(0.7-7) \times 10^{13}$ cm^{-3}) and [DMS] ($(1.5-5) \times 10^{14}$ cm^{-3}). Figure 11 shows an example of the formation and decay of Br−DMS. The [Br−DMS] was calculated by use of $\sigma(390\text{ nm}) = 2.04 \times 10^{-17}$ cm^2 obtained earlier. The form of the profile is similar to that shown in Figure 5 whereby the Br−DMS is formed rapidly and is then removed by reaction 5.

Attempts were made to fit numerically the absorption signals employing a mechanism including reactions 4, −4, 5, 14, and 1. k_4, k_{-4}, k_{14}, and k_1 were fixed at the values obtained in this work. The parameters k_5 and σ(Br−DMS) have the greatest uncertainty, and were allowed to vary to obtain the best possible fit to the experimental data. Figure 11 shows the results of this analysis where the Br-atom yield from reaction 1 was fixed at (i) unit yield (dashed line), (ii) 0.7 yield (solid line), and (iii) no Br-atom formation (broken line). It is noted that the values of k_5 and σ(Br−DMS) returned from the fits were well within the respective uncertainty limits; e.g. for Figure 11 (ii) the fit results were $k_5 = (4.7 \pm 0.4) \times 10^{-10}$ cm^3 s^{-1} and σ(Br−DMS)

$= (1.7 \pm 0.2) \times 10^{-17}$ cm^2 (errors are 2σ). It is clear that the profile is dominated initially by the Br atoms formed in the source chemistry (reactions 4, −4, and 5), but that the Br atoms formed on the longer time scale via reactions 1 and 14a influence the decay at long times. The best fits are given by Figure 11, (i) dashed line, and (ii) solid line, which are difficult to separate given the noise level. We conclude that it is not possible to determine a quantitative branching ratio for reaction 1 from this experiment, but the data do support a lower limit of 0.7 Br-atom yield.

The present yield from direct observation of DMSO of 1.17 ± 0.34 is higher than obtained in previous measurements of the DMSO branching ratio, but it is within the combined uncertainty limits; Bedjanian et al.[14] report 0.94 ± 0.11 from a low-pressure discharge-flow/MS study at 320 K, and Barnes et al.[11] report 0.9 ± 0.2 from an FTIR study in 760 Torr of synthetic air at 298 K. The potential exothermic product channels for reaction 1 are

$$\mathrm{BrO + DMS \rightarrow DMSO + Br} \qquad \Delta H = -128.0 \pm 2.6 \quad (1a)$$

$$\rightarrow \mathrm{CH_3SO + CH_3Br} \qquad \Delta H = -190.8 \pm 19.5 \quad (1b)$$

$$\rightarrow \mathrm{CH_3SBr + CH_3O} \qquad \Delta H = -113 \pm 40 \quad (1c)$$

(values of ΔH_f are taken from ref 7 except CH_3SO (−67 kJ mol^{-1}; estimated via thermochemical data, and we assume 10 kJ mol^{-1} uncertainty)[37] and DMSO;[38] $\Delta H_f(CH_3SBr)$ was obtained using bond additivity rules[39] assuming 10 kJ mol^{-1} error). Channels 1b and 1c require highly strained, four-member transition states which are energetically unfavorable. Indeed, CH_3Br and CH_3SBr were not observed in the FTIR study of Barnes et al.,[11] who place a very conservative upper limit of 10% yield for both products based upon an assessment of detection limits.[40] No information about these potential products is given by Bedjanian et al.[14]

In the present measurement, we are not sensitive to the formation of CH_3SBr and CH_3Br. Comparison of the cross sections of CH_3SBr (4.0×10^{-19} cm^2)[41] and CH_3Br (6.7×10^{-19} cm^2)[41] with DMSO (8.2×10^{-18} cm^2)[36] at 210 nm, shows that a potential 10% yield (based upon the upper limit of Barnes et al.)[40] of either compound would have a negligible (<1%) effect on our absorption profile. The fact that our DMSO yield is greater than unity most likely reflects the systematic error in the DMSO cross sections.

In view of the lack of a positive identification of CH_3SBr and CH_3Br as products of reaction 1, it is concluded that DMSO is the dominant product, with a yield close to unity. Although channels 1b and 1c cannot be ruled out absolutely, they are at most only minor processes, and the scatter in the measured DMSO yields results from the difficulty in calibrating the concentration of a compound that has a high affinity for surfaces.

4. Atmospheric Implications

We have used MOCCA, a chemical box model, to assess the impact of the reaction between BrO and DMS in the marine boundary layer. In the model a constant oceanic flux of DMS is assumed. It reacts with OH, NO_3, Cl, Br, BrO, and IO. A detailed model description can be found elsewhere.[9,10] Here we simulate clean, marine air of the mid-latitudes at the beginning of spring. Bromide from sea-salt particles is converted into reactive forms by multiphase reactions involving HOBr,[42]

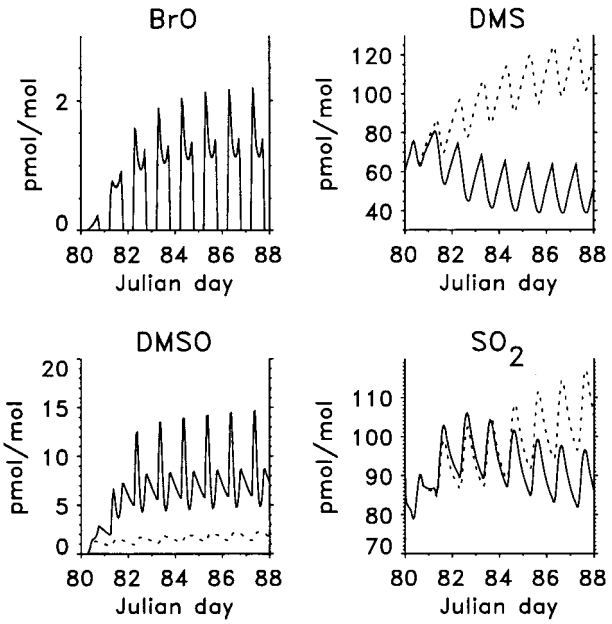

Figure 12. Molar mixing ratios of BrO, CH_3SCH_3 (DMS), $CH_3S(O)CH_3$ (DMSO), and SO_2. Two model runs are shown: one with the reaction DMS + BrO included with a rate constant of 4.4×10^{-13} cm^{-3} (solid line), and one in which the rate constant is set to zero (dotted line). The results for BrO are almost identical for both runs.

resulting in BrO daytime average mixing ratios of slightly above 1 pmol/mol. Model results for BrO, DMS, DMSO, and SO_2 are shown in Figure 12, where they are compared to a sensitivity study in which the reaction of BrO with DMS is switched off. It is clear that BrO is an important sink for DMS. In addition, DMSO, of which the only other important source in MOCCA is the addition of OH to DMS (at 50% yield), is increased considerably. DMSO is lost by scavanging on aerosol, and reaction with OH. The loss of DMS via reaction with BrO therefore reduces the DMS concentration and the rate of its OH-initiated oxidation by SO_2, which is consequently also reduced. The concentration of BrO is not affected as it is regenerated by reaction of Br atoms with O_3:

$$\mathrm{BrO + DMS \rightarrow DMSO + Br} \quad (1a)$$

$$\mathrm{Br + O_3 \rightarrow BrO + O_2} \quad (15)$$

$$\text{net: } \mathrm{DMS + O_3 \rightarrow DMSO + O_2}$$

The net result is a bromine-catalyzed destruction of DMS and O_3, although O_3 concentrations are not affected significantly. As DMS is an important reactant for the NO_3 radical, reduced DMS concentrations also result in increased NO_3 concentrations. This in turn results in enhanced N_2O_5 levels, and increases the rate of $ClNO_2$ formation at night via N_2O_5 reaction with sea-salt. $ClNO_2$ is rapidly photolyzed at dawn to generate chlorine atoms, and the net result is thus an indirect chlorine activation mechanism. To date, there are no measurements of BrO in the remote marine boundary layer over the ocean, as the present detection limit[43] for differential optical absorpion techniques (≈1 pmol/mol) is similar to the expected concentration. We note however that 1 pmol/mol of BrO gives rise to a significant adjustment of the predicted DMS/DMSO ratio, i.e., DMS/DMSO ≥ 100 in the absence of BrO, but is reduced to ≤10 for 1 ppt BrO (see Figure 12). As both DMS and DMSO are expected to be present at concentrations well above their detection limits of ≈1 pmol/mol using selected ion chemical ionization mass spectrometry,[44] simultaneous DMS and DMSO

measurements may provide an indirect means for confirming the presence of BrO in remote marine air masses. We note that there are indications that both the rate of oxidation of DMS[45] and the seasonal variation in the DMSO to methane sulfonic acid ratio[5] (both of which will be perturbed by the presence of BrO) are presently not well understood.

5. Conclusions

We obtained the first "high pressure" value of $k_1 = (4.40 \pm 0.66) \times 10^{-13}$ cm^3 s^{-1} independent of pressure from 60 to 200 Torr N_2 at 295 K. This value is significantly larger than the current recommendation based upon low-pressure flow-tube measurements. By observing the formation of DMSO directly, we obtain a branching ratio of 1.17 ± 0.34 for its yield in reaction 1. The reaction with BrO is a significant sink for DMS and source of DMSO in the marine boundary layer. In addition, we obtained the first values of $k_5 = (4.2^{+2.3}_{-1.2}) \times 10^{-10}$ cm^3 s^{-1} for the fast reaction of Br atoms with the Br−DMS adduct and $\sigma^{365nm}_{max} = (2.74^{+1.6}_{-1.1}) \times 10^{-17}$ cm^2 for the absorption cross sections of the adduct. The uncertainties quoted are based largely upon the potential error associated with laser fluence measurements to obtain $[Br]_o$.

Acknowledgment. Thanks are extended to K-H. Möbus for the *J*-value calculations, A. J. Hynes for supplying DMSO cross sections, and I. Barnes for some helpful discussions. We gratefully acknowledge partial financial support from the MPI-Forschungspreis (Alexander-von-Humboldt Stiftung).

References and Notes

(1) Andreae, M. O. The Emission of Sulphur to the Remote Atmosphere: Background Paper. In *The Biogeochemical Cycling of Sulphur and Nitrogen in the Remote Atmosphere;* Galloway, J. N., et al., Eds.; D. Reidel Publishing Co.: Dordrecht, The Netherlands, 1985; p 5.

(2) Tyndall, G. S.; Ravishankara, A. R. *Int. J. Chem. Kinet.* **1991**, *23*, 483.

(3) Turnipseed, A. A.; Ravishankara, A. R. *The Atmospheric Oxidation of Dimethylsulphide: Elementary Steps in a Complex Mechanism*, *Dimethylsulphide: Oceans, Atmosphere and Climate;* Belgirate: Italy, 1992; p 185.

(4) Cooper, D. J. *J. Atmos. Chem.* **1996**, *25*, 97.

(5) Sciare, J.; Baboukas, E.; Hancy, R.; Mihalopoulos, N.; Nguyen, B. C. *J. Atmos. Chem.* **1998**, *30*, 229.

(6) Barnes, I.; Bastian, V.; Becker, K. H.; Overath, R. D. *Int. J. Chem. Kinet.* **1991**, *23*, 597.

(7) DeMore, W. B.; Sander, S. P.; Golden, D. M.; Hampson, R. F.; Kurylo, M. J.; Howard, C. J.; Ravishankara, A. R.; Kolb, C. E.; Molina, M. J. *Chemical Kinetics and Photochemical Data for use in Stratospheric Modeling*, JPL Publication 97-4; Jet Propulsion Laboratory: Pasadena, CA, 1997.

(8) Toumi, R. *Geophys. Res. Lett*. **1994**, *21*, 117.

(9) Sander, R.; Crutzen, P. J. *J. Geophys. Res.* **1996**, *101*, 9121.

(10) Vogt, R.; Crutzen, P. J.; Sander, R. *Nature* **1996**, *383*, 327.

(11) Barnes, I.; Becker, K. H.; Overath, R. D. *Tropospheric Chemistry of Ozone in the Polar Regions*; NATO ASI Series 1: Global Environmental Change; Niki, H., Becker, K. H., Eds.; 1993, *I 7*, 371.

(12) Maguin, F.; Mellouki, A.; Laverdet, G.; Poulet, G.; Le Bras, G. *Int. J. Chem. Kinet.* **1991**, *23*, 237.

(13) Daykin, E. P.; Wine, P. H. *J. Geophys. Res.* **1990**, *95*, 18547.

(14) Bedjanian, Y.; Poulet, G.; Le Bras, G. *Int. J. Chem. Kinet.* **1996**, *23*, 383.

(15) Le Bras, G. *Tropospheric Chemistry of Ozone in the Polar Regions*; NATO ASI Series 1: Global Environmental Change; Niki, H., Becker, K. H., Eds.; 1993, *17*, 397.

(16) Barone, S. B.; Turnipseed, A. A.; Ravishankara, A. R. *J. Chem. Soc., Faraday Discuss.* **1995**, *100*, 39.

(17) Hynes, A. J. Reaction Mechanisms in Atmospheric Chemistry: Kinetic Studies of Hydroxyl Radical Reactions. In *Advances in Spectroscopy*; Clark, R. H. J., Hester, R. E., Eds.; John Wiley: Chichester, England, 1995; Vol. 24, pp 309−346.

(18) Wine, P. H.; Nicovich, J. M.; Stickel, R. E.; Zhao, Z.; Shackelford, C. J.; Kreutter, K. D.; Daykin, E. P.; Wang, S. NATO ASI Series 1, Global Environmental Change; Niki, H., Becker, K. H., Eds.; 1993, *17*, 385.

(19) Bauer, D.; Ingham, T.; Moortgat, G. K.; Crowley, J. N. *J. Phys. Chem.* **1998**, *102*, 2857.

(20) Mount, G. H.; Warden, E. S.; Moos, H. W. *J. Astrophys.* **1977**, *L47*, 214.

(21) Nesbitt, D. J.; Leone, S. R. *J. Phys. Chem.* **1980**, *73*, 6182.

(22) Talukdar, R. J.; Vaghjiani, G. H.; Ravishankara, A. R. *J. Chem. Phys.* **1992**, *96*, 8194.

(23) Scott, J. D.; Causley, G. C.; Russell, B. R. *J. Chem. Phys.* **1973**, 59, 6577.

(24) Hearn, C. H.; Turcu, E.; Joens, J. A. *Atmos. Environ.* **1990**, *24A* (*7*), 1939.

(25) Maric, D.; Burrows, J. P.; Moortgat, G. K. *J. Photochem. Photobiol.* **1994**, *83*, 179.

(26) Originally cited as a private communication with P. H. Wine in Butkovskaya, N. I.; Le Bras, G. *J. Phys. Chem.* **1994**, *98*, 2582.

(27) Curtis, A. R.; Sweetenham, W. P. *FACSIMILE*, AERE Harwell publication R 12805; Computer Science and Systems Division, Harwell Laboratory: Oxfordshire, U.K., 1987.

(28) Jefferson, A.; Nicovich, J. M.; Wine, P. H. *J. Phys. Chem.* **1994**, *98*, 7128.

(29) Baulch, D. L.; Duxbury, J.; Grant, S. J.; Montague, D. C. *J. Phys. Chem. Ref. Data*, 10, Suppl. **1981**.

(30) Wahner, A.; Ravishankara, A. R.; Sander, S. P.; Friedl, R. R. *Chem. Phys. Lett.* **1988**, *152*, 507.

(31) LUTHER program (adapted from Luther, F. M.; Gelinas, R. J. *J. Geophys. Res.* **1976**, *81*, 1125. Isaksen, I. S. A.; Midtbo, K.; Crutzen, P. J.; Institut Report Series, No. 20, Institut for Geofysikk, University of Oslo, 1976).

(32) Nicovich, J. M.; Wine, P. H. *Int. J. Chem. Kinet.* **1990**, *22*, 379.

(33) Timonen, R. S.; Seetula, J. A.; Gutman, D. *J. Phys. Chem.* **1990**, *94*, 3005.

(34) Chow, Y. L.; Bakker, B. H. *Can. J. Chem.* **1982**, *60*, 2268.

(35) Hynes, A. J.; Pounds, A. J.; McKay, T.; Bradshaw, J. G.; Wine, P. H. Detailed mechanistic studies of the OH-initiated oxidation of biogenic sulfur compounds under atmospheric conditions, presented at 12th Int. Symp. on Gas Kinet., Reading, England, 1992.

(36) Hynes, A. J.; Wine, P. H. *J. Atmos. Chem.* **1996**, *24*, 23. Cross section data supplied by A. J. Hynes in a private communication.

(37) Atkinson, R.; Baulch, D. L.; Cox, R. A.; Hampson, R. F.; Kerr, J. A.; Troe, J. *J. Phys. Chem., Ref. Data.* **1992**, *21*, No. 6.

(38) *Handbook of Chemistry and Physics*; Lide, D. R., Ed.; CRC Press: New York; 1997, p *78*.

(39) Benson, S. W. *Thermochemical Kinetics*; Wiley: New York, 1976.

(40) Barnes, I. Private communication.

(41) Unpublished data from this laboratory.

(42) Fickert, S.; Adams, J. W.; Crowley, J. N. Activation of Br_2 and BrCl via uptake of HOBr onto aqueous salt solutions. *J. Geophys. Res.*, in press.

(43) Tuckermann, M.; Ackermann, R.; Gölz, C.; Lorenzen-Schmidt, H.; Senne, T.; Stutz, J.; Trost, B.; Unold, W.; Platt, U. *Tellus* **1997**, *49B*, 533.

(44) Berresheim, H.; Huey, J. W.; Thorn, R. P.; Eisele, F. L.; Tanner, D. J.; Jefferson, A. *J. Geophys. Res.* **1998**, *103*, 1629.

(45) Yvon, S. A.; Saltzman, E. S.; Cooper, D. J.; Bates, T. S.; Thomson, A. M. *J. Geophys. Res.* **1996**, *101*, 6899.